

# Discontinuum–Equivalent Continuum Analysis of the Stability of Tunnels in a Deep Coal Mine Using the Distinct Element Method

Srisharan Shreedharan<sup>1</sup> · Pinnaduwa H. S. W. Kulatilake<sup>1</sup>

Received: 28 May 2015 / Accepted: 27 October 2015 / Published online: 9 November 2015  
© Springer-Verlag Wien 2015

**Abstract** An imperative task for successful underground mining is to ensure the stability of underground structures. This is more so for deep excavations which may be under significantly high stresses. In this manuscript, we present stability studies on two tunnels, a horseshoe-shaped and an inverted arch-shaped tunnel, in a deep coal mine in China, performed using the 3DEC distinct element code. The rock mass mechanical property values for the tunnel shapes have been estimated through a back-analysis procedure using available field deformation data. The back-analysis has been carried out through a pseudo-time dependent support installation routine which incorporates the effect of time through a stress-relaxation mechanism. The back-analysis indicates that the rock mass cohesion, tensile strength, uniaxial compressive strength, and elastic modulus values are about 35–45 % of the corresponding intact rock property values. Additionally, the importance of incorporating stress relaxation before support installation has been illustrated through the increased support factor of safety and reduced grout failures. The calibrated models have been analyzed for different supported and unsupported cases to estimate the significance and adequacy of the current supports being used in the mine and to suggest a possible optimization. The effects of supports have been demonstrated using deformations and yield zones around the tunnels, and average factors of safety and grout failures of the supports. The use of longer supports and floor bolting has provided greater stability for the rock masses

around the tunnels. Finally, a comparison between the two differently shaped tunnels establishes that the inverted arch tunnel may be more efficient in reducing roof sag and floor heave for the existing geo-mining conditions.

**Keywords** Tunnel stability · Deep coal mine · Numerical modeling · Back-analysis · Support optimization · 3DEC

## 1 Introduction

Coal mining in China is predominantly an underground activity, with about 95 % of the coal workings existing below ground (China Coal Society Open Pit Mine Committee 2010). Additionally, the fact that coal has served as the major source of energy in China has forced mines to expand their production and go deeper underground in search of better quality and higher quantities (He and Song 2012). With deeper underground excavations, the associated in situ stresses increase and the strata ‘squeezes’ the excavated span. This is particularly dangerous and is associated with a higher number of reported incidents of roof collapse. As of 2008, roof fall is responsible for the highest number of coal mine deaths in China, numbering at about 1200 deaths in 2008 (The Compiling Committee of China 2010).

Currently, extraction depths of 600 m and higher continue to be the norm, with at least 20 coal mines having excavations at 1000 m or more below ground (Huang 2008). At these depths, the rock mass is under very high in situ stress fields and extremely prone to rock bursts. Apart from this, the issues of excessive temperature, water inrush, gas explosions in case of highly gassy mines, and general geological complexity associated with depth are the important parameters to be dealt with when discussing

✉ Pinnaduwa H. S. W. Kulatilake  
kulatila@u.arizona.edu; kulatila@email.arizona.edu

<sup>1</sup> Rock Mass Modeling and Computational Rock Mechanics Laboratories, University of Arizona, Tucson, AZ 85721, USA

about the structural stability of deep excavations. Since roof collapse is a major cause of accidents, it is important that it be controlled. Excavations under high in situ stresses also undergo significant plastic deformations. This is further aggravated when the strata in consideration is a soft formation such as coal-measure formations. Controlling this excessive deformation is imperative and is usually carried out using different supports such as bolts, cables, wire meshes, and shotcreting. The various supports, installation techniques, performance and advancements in support technology are described by Peng and Tang (1984), Hoek et al. (2000), Mark and Barczak (2000), and Aldorf and Exner (2013) among others.

The Xiezhuang coal mine, located in the Xinwen coal mining area (Fig. 1), is one of the deeper coal mines in China, with excavations at depths exceeding 1300 m. Two of the many development tunnels in this mine are used for the numerical analyses presented in this paper. The tunnels are driven in a soft sandy shale stratum. It has been predicted that the tunnels will not pass through any significant discontinuity structure such as faults or water-bearing rock. The rock mass has three discontinuity sets with the most distinct being a set of horizontal to near horizontal bedding planes. The tunnels, due to them being driven in soft shale, experience significant floor heaving.

To observe the response of the rock mass surrounding the tunnels and of the support system used in the mine, the 3DEC distinct element code (Itasca 2008) has been used to build models of the tunnels. Subsequently, a back-analysis routine has been performed to calibrate the rock mass properties using the available deformation data from the mine. Finally, different support designs have been implemented on the calibrated model to determine the best support design. Also included are analyses of models without supports, to show the effect of supports on plastic deformation. In all cases, the effect of ground response on supports has been explicitly modeled using the concept of ground reaction curves (Brown et al. 1983), and a safety

factor-based approach to study cable bolt stability in 3DEC has been introduced.

## 2 Previous Studies on Tunnel Stability Using Numerical Modeling

Most rocks in nature contain planes which divide the rock mass into smaller intact rocks. These discontinuities are planes where a change in physical, mechanical, or chemical properties of the rock mass can be observed (Price 2008). Discontinuities may be fractures, fissures, joints, faults, folds, dykes, or bedding planes. While discontinuities are of many types, they generally occur as planes of weakness where the likelihood of fracture is highest, when subjected to a stress. Hence, they are of significance when the stability of an underground excavation is to be estimated. The most commonly observed discontinuity type in underground excavations is a joint or joint set(s) and is characterized by parameters such as joint set number, joint orientation, joint size, joint frequency, joint roughness parameters, joint normal stiffness, joint shear stiffness, and joint strength parameters. While these joints have a significant influence on the stability of underground and surface excavations, quantitatively observing this influence can prove to be complex.

With the advent of powerful computers in tandem with advances in mathematics, several numerical modeling methods have been introduced to compute the stability of excavations. Many of these modeling methods are able to incorporate the complex interactions between excavations and discontinuities to varying degrees of accuracy. The methods can be broadly categorized as being continuum methods, discontinuum methods, or hybrid methods (Elmo 2006).

As their names may indicate, the continuum methods do not explicitly define joints and instead allow discontinuous interactions through interface/joint elements. Conversely, the discontinuum methods fundamentally model a rock mass as an assemblage of rigid or deformable intact rock blocks with explicit discontinuity interfaces separating them. Some of the popular continuum methods include the boundary element method (BEM), the finite element method (FEM), and the finite difference method (FDM). Deb and Das (2010) state that joint elements commonly available in finite element software packages cause numerical inconsistencies which seem to depend on the boundary conditions, problem geometry, and the accuracy of the computer used, thus opening the doors for further research into developing better joint elements which can do away with these drawbacks. Cundall (2001) also stresses on the use of discontinuum methods over continuum methods for simulating rock and soil particles as

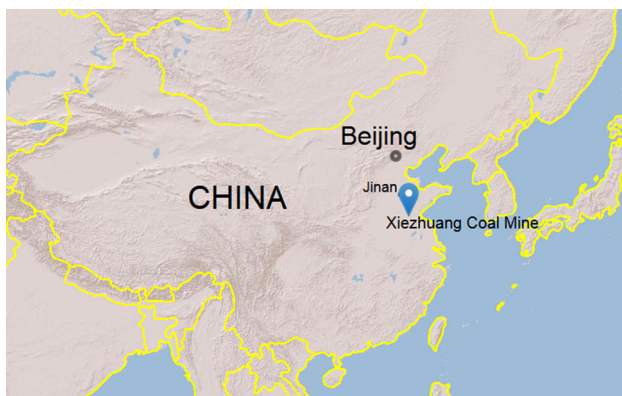


**Fig. 1** Geographical location of the Xiezhuang coal mine

continuum methods do not handle particle fracturing/rupturing and large displacements and large rotations. Hence, discontinuum methods such as the distinct element method (DEM) proposed by Cundall (1971) and the discontinuous deformation analysis (DDA) by Shi and Goodman (1985) may be more appropriate for handling the behavior of jointed rocks.

The DEM models rock masses as a cluster of blocks which may be rigid or deformable and an explicit solution procedure is employed. The blocks are allowed to behave as continuum media and the block and joint interactions are modeled by the Newton's laws of motion. This eliminates the need for a large stiffness matrix unlike the FEM. The superiority of DEM for modeling discontinuous rock masses has been explained by Fairhurst and Pei (1990), where the authors compare the results obtained by a FEM and a UDEC model of an excavation in a jointed rock mass. Barla and Barla (2000) also compare the continuum and discontinuum approaches and conclude that, despite its relatively unproven nature at the time of publication, 3DEC and other DEM-based packages perform a better job of accurately simulating jointed rock masses. They stress that the only constraint to its widespread use would be the requirement for superior computer hardware. However, since 2000, there have been many improvements in computing systems and this no longer remains a significant constraint. Yuyong and Jian (2004) have successfully employed UDEC and 3DEC to perform a dynamic study on the response of discontinuous rocks to explosions underground. Hao and Azzam (2005) and Vardakos et al. (2007) have performed 2D discontinuum modeling of tunnels in different rock types, using UDEC. A 3D stress analysis using 3DEC, coupled with an equivalent continuum analysis, for a mine tunnel in an underground iron ore mine was performed by Wang et al. (2012), with encouraging results which correlated well with observed field deformations. Wu and Kulatilake (2012) investigated the stability of a tunnel at a dam site in China using three-dimensional discontinuum and equivalent continuum numerical modeling techniques. The DEM has also been employed to perform a structural stability analysis of theoretical designs of a sculpture in an underground cavern in the Canary Islands (Macklin et al. 2012). This is a classic example of the usefulness of numerical modeling before the actual commencement of the project as it helped eliminate those designs which may have led to a collapse of the cavern system.

The DDA can be used to model large displacements and block failure in deformable systems. The method, similar to the FEM, is derived using the principle of minimum potential energy. This is the fundamental difference between the DDA, which uses implicit energy based solution schemes, and the DEM code which uses explicit

force based procedures. Wu et al. (2005) most recently proposed a code for 3D DDA analysis and demonstrated its usefulness for analyzing a rock slope's stability against toppling in Japan. According to MacLaughlin and Doolin (2006), the DDA has been popularly used by rock mechanics experts for analysis of rock structure stability, especially in cases of slope and dam stability, and for underground caverns. Shi (2014) has also used the DDA for the stability analysis of underground caverns, in addition to the stability of slopes, using 2D DDA and a simplified 3D DDA. Its usefulness for the analysis of toppling of slopes has been stressed upon by Shi (2007). Jian-ping et al. (2012) modified the original DDA code to include the potential energy due to rock bolts for optimizing the support requirements for the large deformations observed in a mine tunnel. The primary arguments in favor of the use of DDA, as put forth by Cheng (1998), are that the DEM method requires artificial springs to absorb the energy generated, to achieve equilibrium, and that the explicit time marching algorithm used by the DEM can cause numerical instability if very small time steps are not used. These issues with DEM are now relatively obsolete due to the availability of significantly higher computational capacities. In addition, due to its non-commercialization, DDA is available as a freeware. In contrast, the DDA has a multitude of drawbacks of its own. Scheldt (2003) discovered that if a model geometry is such that there is a large ratio between rock blocks, or if joints have nearly zero angle between them, the computation fails. Also, stresses within a block are assumed to be constant, blocks cannot undergo fracture, pore pressure has not been considered, and the post-processing capabilities of the available DDA code are limited, as opposed to a wide variety of options available in commercial DEM codes. A limitation of the DDA, which has been repetitive throughout literature, is the problem of numerical truncation and loss of significant effective digits (Ma 1999; Zhao et al. 2011; Ohnishi et al. 2014).

The Hybrid methods, as the name would indicate, attempt to take the best of both continuum and discontinuum methods. Two of the popular hybrid codes incorporating FEM/DEM, used for rock mass simulations, are Elfen (Rockfield 2011) and YGeo (Mahabadi et al. 2012). Munjiza et al. (1995) elucidated the inherent issues in computing power which could be a deterrent for the FEM/DEM methods from gaining popularity in the near future. Progressive failure in rock slopes was modeled using a 2D hybrid FEM/DEM approach by Eberhardt et al. (2003). Elmo (2006) used the Elfen code to determine the strength of a fractured rock mass. The modeling was further carried out on a 3D version of Elfen. Advances in computing and parallel processing have seen advancements in FEM/DEM codes as well. Recent versions of Elfen have been used to study fractured rock pillars in a limestone mine and surface

subsidence due to block caving (Elmo and Stead 2010; Vyazmensky et al. 2010). Elmo et al. (2013) and Hamdi et al. (2014) used Elfen to model fractures in laboratory testing of specimens. Lisjak et al. (2014) presented a 2D FEM/DEM analysis exploring the failure mechanisms of unsupported circular tunnels in clay shales. Coggan et al. (2012) provide a comprehensive compilation of the advantages and drawbacks of the various methods currently being used for numerical modeling of complex rock engineering problems.

Significant numerical work on deep mining in soft rock has been undertaken in China. Kang et al. (2014) have attempted to tackle the problem of floor heave in coal under high in situ stress using FLAC3D (a finite difference code) and introduce a new supporting mechanism for floor reinforcement. The stability of a haul road in a deep coal mine has been studied using finite element techniques by Shan et al. (2005), and a 2D distinct element analysis has been performed by Xiao et al. (2011). However, supports have not been explicitly incorporated into the models and the effect of time dependent stress relaxation between excavation and support installation is not considered. Taking into consideration the various strengths and limitations of available modeling frameworks, 3DEC has been selected for the current study as it is a tried and tested code capable of satisfactorily modeling tunnel stability by explicitly incorporating discontinuities and stress anisotropy. The time dependence of support installation has also been modeled implicitly using the concept of ground reaction curves.

### 3 Development of the Numerical Model

The numerical model is a cuboid of dimensions 50 m × 57 m × 50 m with gravity acting along the negative z-axis. The coordinate system has its origin at the center of the tunnel such that the x-coordinate axis ranges from −25 to 25 m, y-coordinate axis ranges from 0 to 57 m, and the z-coordinate axis ranges from −23 to 27 m. To fully capture the effect of supporting on the deformation, failure zone and stress redistribution in a deep tunnel in soft rock, a total of ten cases have been considered with various modeling and supporting schemes. This includes modeling two tunnel shapes as unsupported, bolted on roof and ribs, and bolting on roof, ribs, and floor. The two shapes explored in this study are a conventional horseshoe shape and an inverted arch shape both of which have been excavated in the mine. The shapes and dimensions of the tunnels are shown in Fig. 2, which also serves as a schematic for the unsupported models. Figures 3 and 4 show the different supported cases, i.e., the cases without and with floor bolting, respectively. A compilation of the

variations in the different cases is laid out in Table 1. It should be noted that cases 4 and 9, and Fig. 3 represents the actual scheme of working present in the mine. The dotted and solid lines in Figs. 3 and 4 represent the first and second supports.

The numerical model itself has been created with the actual lithologies observed in the field. The model runs 57 m along the tunnel axis. The supports used are cable bolt elements as available in 3DEC for both the first and second supports. The in-plane spacing between two bolts of the same type is 0.8 m, which is also the out-of-plane spacing into the tunnel axis. Between any two bolts, the spacing in-plane and out-of-plane is 0.4 m. The second supports are installed along the tunnel axis such that they are placed at the center of the square formed by connecting any four adjacent first supports. The tunnel runs at a depth of about 1325 m from the surface and the model dimensions have been selected to ensure that there is sufficient material around the tunnel. This is essential to ensure that the model boundary is farther than the area of influence. As a general guideline, the horizontal and vertical dimensions of the model should be at least five times the horizontal and vertical dimensions of the tunnel. In the current set-up, the cross-section dimensions of 50 m × 50 m sufficiently satisfy this guideline.

The tunnel is approximately horizontal, as are the interfaces between different lithologies and the explicitly modeled bedding planes. The in situ stresses are made available from the mine at three different depths all of which are shallower than 1300 m. Hence, the horizontal in situ stresses used in the model are estimated by interpolating the three available data points. The vertical stress at 1300 m has been estimated as a function of depth using a constant average overburden density of 2650 kg/m<sup>3</sup>, to be 34.5 MPa. The collected in situ stress data are given in Table 2.

The anomaly at depth 1150 m has been attributed to a fault zone at about 1150 m, and the data point was ignored while estimating the horizontal stresses at 1300 m. The data points at 790 and 1071 m were used to estimate the lateral stress ratios at those depths as given in Eqs. (1) and (2). Using these stress ratios, the maximum and minimum horizontal stresses at 1300 m were estimated as being 50.8 and 26.2 MPa, respectively:

$$K_{01} = \frac{\sigma_{Hmax}}{\sigma_v}, \quad (1)$$

$$K_{02} = \frac{\sigma_{hmin}}{\sigma_v}, \quad (2)$$

where  $K_{01}$  and  $K_{02}$  are the maximum and minimum lateral stress ratios,  $\sigma_v$  is the vertical stress (MPa), and  $\sigma_{Hmax}$  and  $\sigma_{hmin}$  are the maximum and minimum horizontal stresses, respectively (MPa).

**Fig. 2** Dimensions of the **a** horseshoe tunnel and **b** the inverted arch tunnel

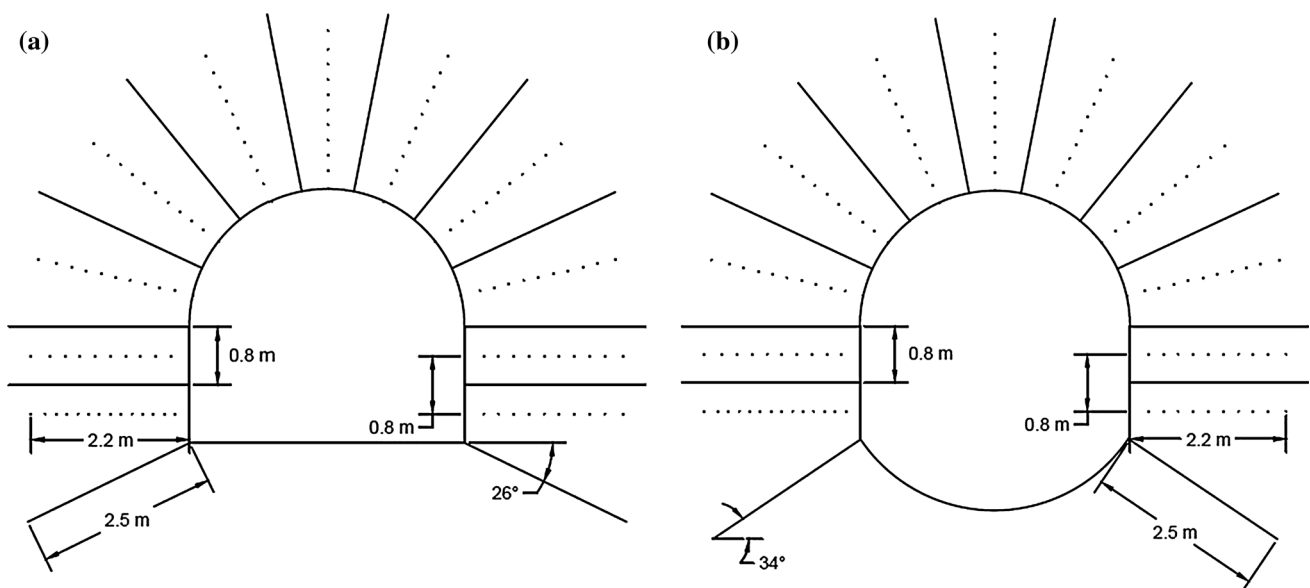
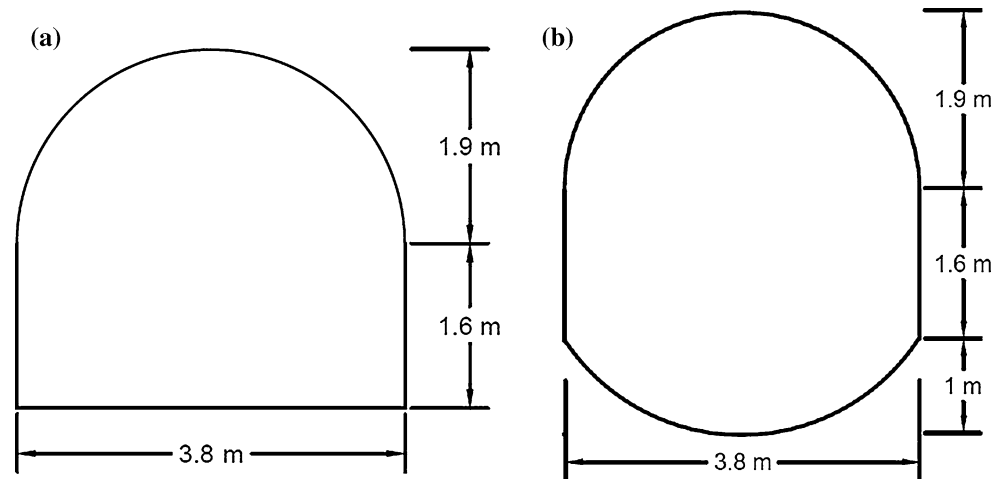


**Fig. 3** Dimensions and orientation of the roof and wall bolting in the **a** horseshoe tunnel and **b** inverted arch tunnel (dotted lines first support, solid lines second support)

The various lithologies incorporated into the model are shown in Fig. 5 and are as observed in the field. It may be noted that the tunnel axis at the mine site was oriented along the direction of the maximum horizontal principal stress, i.e., along the  $y$ -axis direction in the 3DEC model. Hence, the model has been built keeping this as the reference coordinate system. The calculated in situ stress values were applied at the top of the model, i.e., at 1300 m, and the gravitational gradient has been applied to ensure that all components of the stress increase along the depth of the model.

The physical and mechanical properties of intact rock used in the model are given in Table 3. The used intact rock constitutive model is the Mohr–Coulomb elastic-perfectly plastic model. The model is bounded at the base by fixities which prevent vertical movement, and stress

boundaries have been used along the other five faces, with magnitudes equal to the in situ stresses and gradients (if any) along the respective directions. A 2D schematic of the applied boundary conditions is presented in Fig. 6.

The interfaces and bedding planes are described by the Coulomb Slip model given in Eq. (3). The interface mechanical property values have been estimated using the framework given by Kulatilake et al. (1992) and Kulatilake et al. (1993) and are presented in Table 4. Also included in Table 4 are the mechanical property values for the bedding planes incorporated into the second sandy shale stratum (SS2). The discretized model of the two tunnel shapes, i.e., the horseshoe-shaped and inverted arch-shaped tunnels, after incorporating the bedding planes, are presented in Fig. 7. The bedding planes are spaced 1 m apart.



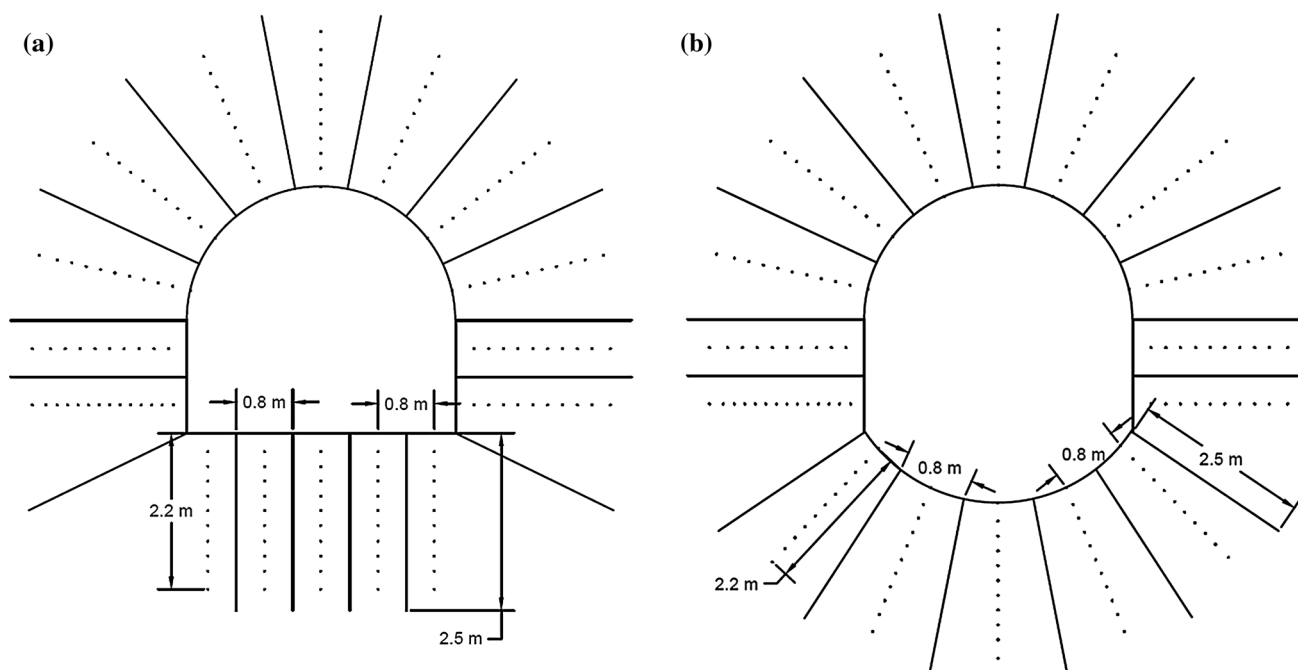


**Fig. 4** Dimensions and orientation of the floor bolting in the **a** horseshoe tunnel and **b** inverted arch tunnel (*dotted lines* first support, *solid lines* second support)

**Table 1** Details of various cases analyzed

Case	Tunnel shape: horseshoe (HS)/inverted arch (IA)	Support installation routine: instantaneous (I)/stress relaxation (SR)	Roof and wall bolting (Y/N)	Floor bolting (Y/N)
1	HS	Unsupported	Unsupported	Unsupported
2	HS	I	Y	N
3	HS	I	Y	Y
4	HS	SR	Y	N
5	HS	SR	Y	Y
6	IA	Unsupported	Unsupported	Unsupported
7	IA	I	Y	N
8	IA	I	Y	Y
9	IA	SR	Y	N
10	IA	SR	Y	Y

**Table 2** In situ stress data for the region

Depth (m)	Vertical stress (MPa)	Maximum horizontal principal stress (MPa)	Minimum horizontal principal stress (MPa)	Direction of maximum horizontal principal stress (MPa)
790	20.9	32.4	16.6	N33.5°E
1071	28.4	39.8	20.6	N39.7°E
1150	30.5	34.6	17.9	N12.5°E

$$\tau = \sigma \tan \phi, \quad (3)$$

where  $\tau$  is the joint shear stress (MPa),  $\sigma$  is the joint normal stress (MPa), and  $\phi$  is the joint friction angle (deg).

The property values of cables, as used in the model, are given in Table 5. In many mines in India and China, a prevalent practice is to make use of discarded haulage

**Fig. 5** Lithologies found at the site

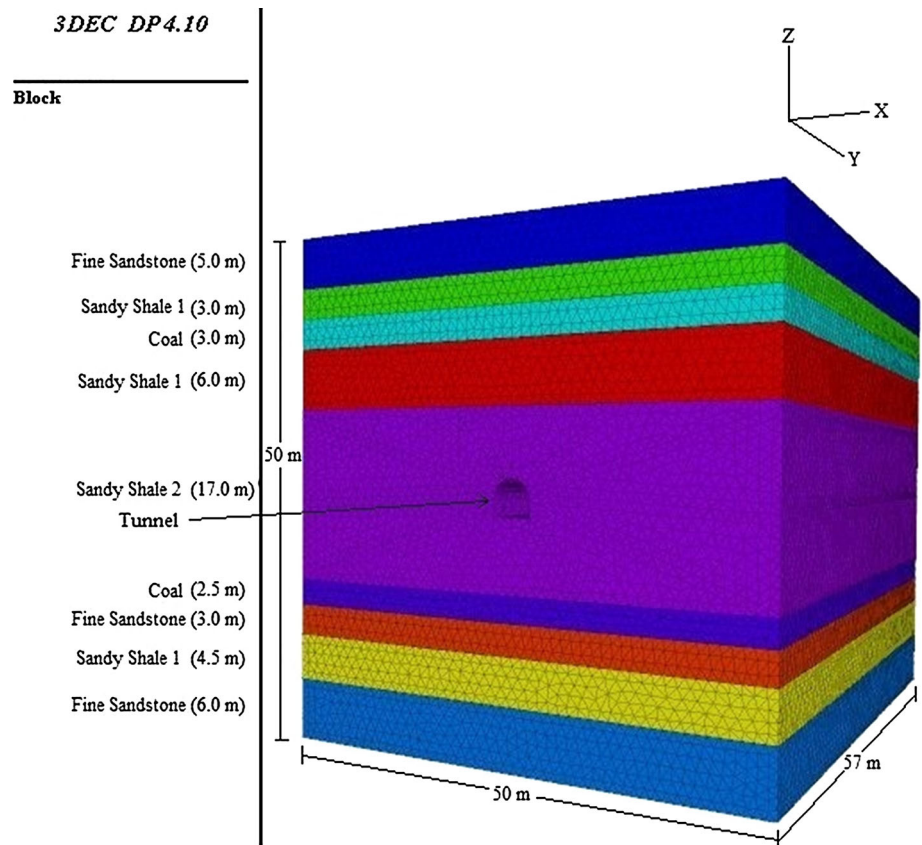


**Table 3** Physical and mechanical property values of the different intact rock types used in the model

Layer	Density (kg/m <sup>3</sup> )	Elastic Modulus (GPa)	Poisson's ratio	Cohesion (MPa)	Internal friction angle	Tensile strength (MPa)	Uniaxial compressive strength (MPa)
Fine sandstone (FS)	2670	35.6	0.17	28.0	36.5	7.0	111.6
Sandy shale 1 (SS1)	2660	26.5	0.29	16.0	32.0	3.8	57.5
Sandy shale 2 (SS2)	2500	25.4	0.32	13.0	27.0	3.2	49.0
Coal (C)	1392	3.0	0.36	2.8	24.0	1.0	8.5

ropes and shaft pulley wire ropes for bolting as a cost saving measure. Due to the presence of grease and lubricants on these wire ropes and due to the fact that they have been subjected to multiple loading and unloading cycles during their operational life, these wire ropes have a reduced adhesion to the grout (Singh et al. 2001). Hence, a bond quality index of 0.45 has been used in this study to account for this phenomenon. This essentially means that the cables perform with 45 % efficiency.

The rock mass constitutive law used in this study is the Mohr–Coulomb strength criterion given in Eq. (4), with tension cut-off.

$$\sigma_1 = UCS + \sigma_3 \left( \tan \left( 45^\circ + \frac{\phi}{2} \right) \right)^2, \tag{4}$$

where  $\sigma_1$  and  $\sigma_3$  are the maximum and minimum principal stresses (MPa), UCS is the uniaxial compressive strength of the intact rock (MPa), and  $\phi$  is the internal friction angle of the rock sample (deg).

To estimate the rock mass properties, the technique of strength reduction has been applied. The intact rock strength is initially used to calculate the deformations and the strength parameter values are systematically reduced until the deformations observed in the model match the field measurements (Table 6). During the strength reduction, the density and intact rock friction angle were kept unchanged since they do not significantly change for a rock mass (Kulatilake et al. 2004). All other strength parameters and Young's modulus were reduced, and the Poisson's ratio was increased. The strength reduction was

implemented using a binary searching algorithm where the strength parameter values were halved after each iteration and the deformations were compared against field measurements. This exercise was carried out until the roof and floor deformations in 3DEC came close to the observed field deformations.

### 4 Results and Discussions

In all the analyses, the deformations and stresses have been plotted at the central vertical plane having  $y = 28.5$  m. To validate the created model and test for inconsistencies, a model without the bedding planes was created since the presence of joints cutting across an excavation can make the analysis of the stress fields around the excavation a confusing or complicated task. Once the validity of this model was established, the bedding planes were incorporated into the model. Figure 8 shows the  $zz$  and  $xx$  stress fields around the horseshoe tunnel. As can be seen, the vertical stress ( $zz$  stress) approaches zero on the roof and floor, and peaks at the walls. Similarly, the horizontal stress ( $xx$  stress) approaches zero on the walls and peaks at the roof and floor. Also, the far field horizontal and vertical stresses are equal to the applied in situ stress field. This confirms that the created model has the right stress fields being applied to it. It may be noted that 3DEC recognizes the compressive stresses/forces as being negative.

The strength reduction-based calibration was carried out using two procedures, i.e., excavation and instantaneous supporting, and delayed supporting. The delay in

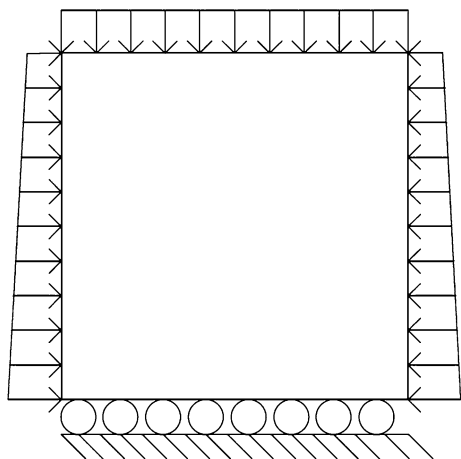


Fig. 6 Boundary conditions applied to the model

Table 4 Discontinuity mechanical property values used in the model

Discontinuity	Type	Friction angle (deg)	Cohesion (MPa)	Tensile strength (MPa)	Joint shear stiffness, JKS (GPa/m)	Joint Normal stiffness, JKN (GPa/m)
FS/SS1	I	34.3	16	0	1063	2736
SS1/SS2	I	29.5	13	0	828	2133
SS2/C	I	25.5	2.8	0	447	1150
FS/C	I	30.3	2.8	0	675	1738
SS1/C	I	28.0	2.8	0	474	1220
SS2	B	16.0	0	0	8	21

I interface, B bedding planes

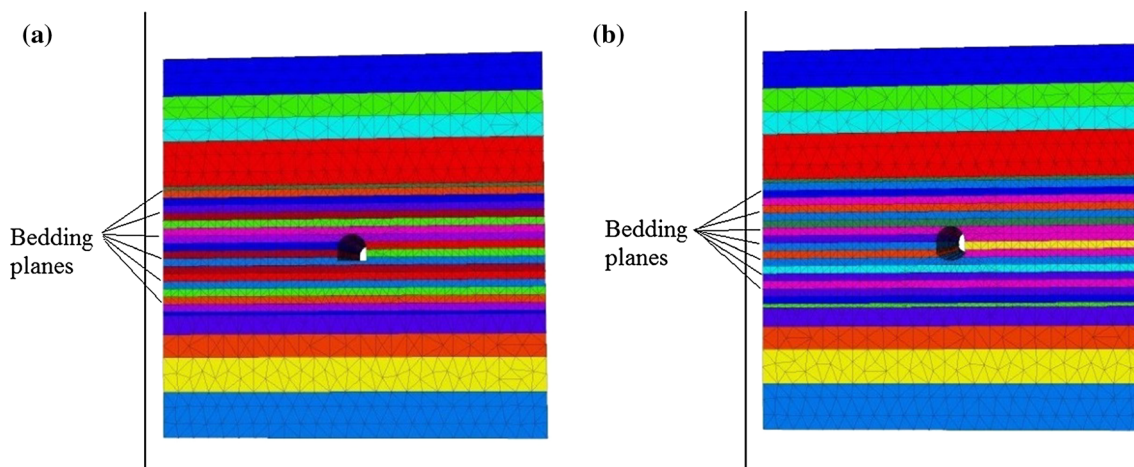


Fig. 7 Model of a horseshoe tunnel and b inverted arch tunnel with bedding planes



**Table 5** Mechanical property values of supports used in the model

	First support	Second support
Young's modulus of bolt (GPa)	98	98
Cable diameter (mm)	15.7	18.3
Cable cross-sectional area (mm <sup>2</sup> )	193.5	262.9
Tensile yield capacity of bolt (MN)	0.28	0.35
Grout cohesive capacity per unit length (MN/m)	0.9	1.04
Grout stiffness per unit length (MN/m/m)	18,674	19,057

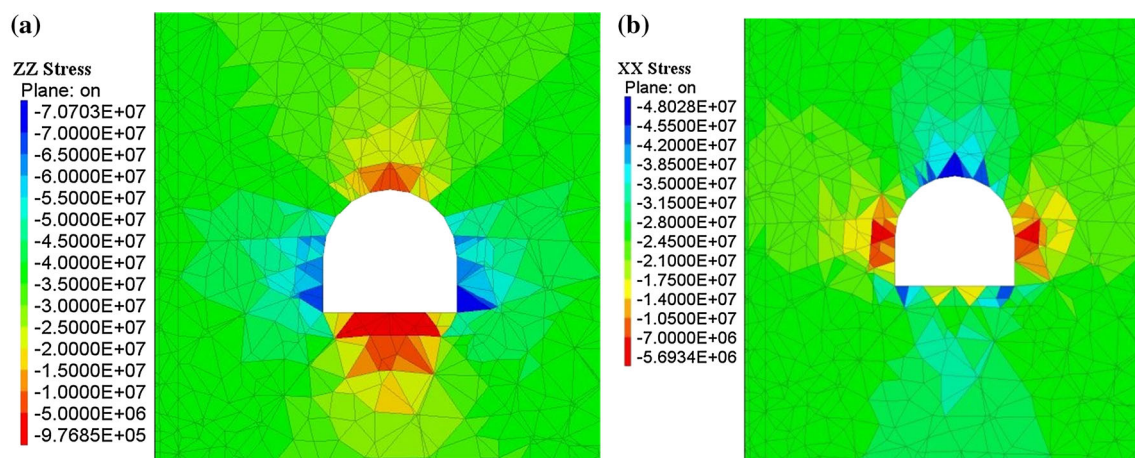
**Table 6** Deformation data at the monitoring point in the mine

Tunnel type	Roof (mm)	Wall (mm)	Floor (mm)
Horseshoe	34	24	52
Inverted arch	44	32	50

supporting has been carried out using a stress relaxation mechanism as opposed to explicit time delay because in the 3DEC environment, time cannot be equated in any way to actual physical time in the field. The stress relaxation has been carried out using the approach detailed in Vardakos et al. (2007) for the UDEC code. In this method, the material is excavated and stresses are applied at the excavation boundary to perfectly balance internal forces. Subsequently, the applied stresses are gradually reduced, the supports are installed after the rock mass has undergone sufficient yielding, applied stresses are completely removed, and the model is allowed to attain an equilibrium state. Ideally, the reduction of stresses must be quasi-static and this comes at a cost of computation time. Hence, in this study, it has been reduced in 10 % increments. A parameter which is seemingly arbitrary is the amount of yielding that the rock mass undergoes between the completion of excavation and installation of supports. This largely depends on the strength properties of the rock and the

stand-up time. Generally, most mines in Asia follow a shift cycle of 8 h, and it has been considered reasonable to assume that the excavated span would have been left unsupported for a period of 8 h. Hence, the yielding is a function of the stress relaxation undergone by the unsupported tunnel during this 8 h period. Ghee et al. (2006) and Vardakos et al. (2007) provide some guidelines on selecting the right numbers for this stress relaxation and a 50 % relaxation has been considered for this study due to the strata being soft sandy shale. This is based on comparison of the rock mass strength in this study with the rock mass strengths in studies by Ghee et al. (2006) and Vardakos et al. (2007). The results of both calibration approaches for the two tunnels are presented in Tables 7, 8, 9, and 10.

It was observed that the calibrated rock mass strength for both the horseshoe and inverted arch tunnel regions was between 37.5 and 43.75 % of intact rock (see Figs. 17, 18 given later). Hence, for the mine at 1325 m, a range of 35–45 % can be considered appropriate, to account for the inherent strength variability present in rocks. Table 11 gives the various mechanical properties for the system considering an average 40 % of intact rock properties. Figure 9 shows the ground reaction curves for the roof, wall, and floor for both tunnel types at 37.5 % intact strength.

**Fig. 8** Horseshoe tunnel without bedding planes showing **a** zz stress distribution and **b** xx stress distribution (unit: Pa)

**Table 7** Calibration of rock mass parameters for HS tunnel with instantaneous support installation

Iteration	Percentage of intact	Deformations (mm)			Factor of safety		Grout bond failure (%)	
		Roof (mm)	Wall (mm)	Floor (mm)	First support	Second support	First support	Second support
1	100	8.9	4.7	11.8	3.67	2.79	2.02	3.58
2	50	26	20.5	33	1.18	1.27	11.11	10.39
3	25	74.5	79.5	93.4	1.02	1.05	19.11	13.67
4	37.5	41	37	51	1.02	1.11	11.86	9.57
5	43.75	32.5	27	41	1.04	1.16	11.22	10.10

**Table 8** Calibration of rock mass parameters for IA tunnel with instantaneous support installation

Iteration	Percentage of intact	Deformations (mm)			Factor of safety		Grout bond failure (%)	
		Roof (mm)	Wall (mm)	Floor (mm)	First support	Second support	First support	Second support
1	100	8.7	5.5	9.3	3.77	2.68	2.02	2.58
2	50	26	22.5	31	1.22	1.24	12.34	10.99
3	25	78.5	88	98.8	1.01	1.06	17.39	17.95
4	37.5	42	41	50.5	1.01	1.11	12.73	11.31

**Table 9** Calibration of rock mass parameters for HS tunnel with stress relaxation and support installation

Iteration	Percentage of intact	Deformations (mm)			Factor of safety		Grout bond failure (%)	
		Roof (mm)	Wall (mm)	Floor (mm)	First support	Second support	First support	Second support
1	100	8.9	4.8	11.9	4.58	4.07	0.69	0.09
2	50	25.7	19.8	32.1	1.36	1.42	10.12	9.94
3	25	78.8	86.5	97	1.02	1.05	19.34	14.9
4	37.5	40.2	35.7	47.8	1.06	1.18	11.21	10.95
5	43.75	31.9	26.6	39.3	1.14	1.25	11.01	11.5

**Table 10** Calibration of rock mass parameters for IA tunnel with stress relaxation and support installation

Iteration	Percentage of intact	Deformations (mm)			Factor of safety		Grout bond failure (%)	
		Roof (mm)	Wall (mm)	Floor (mm)	First support	Second support	First support	Second support
1	100	8.7	5.4	9.2	5.18	4.53	0	0.05
2	50	26.5	22.7	31.3	1.39	1.34	10.19	11.54
3	25	81.2	93	102.7	1.02	1.07	20.37	18.84
4	37.5	42.5	42	51	1.09	1.17	13.2	12.2

**Table 11** Calibrated rock mass property values for the Xiezhuang mine at 1325 m

Layer	Density (kg/m <sup>3</sup> )	Elastic modulus (GPa)	Poisson's ratio	Cohesion (MPa)	Internal friction angle	Tensile strength (MPa)	Uniaxial compressive strength (MPa)
Fine sandstone (FS)	2670	14.2	0.21	11.2	36.5	2.8	44.6
Sandy shale 1 (SS1)	2660	10.6	0.36	6.4	32.0	1.5	23.0
Sandy shale 2 (SS2)	2500	10.2	0.40	5.2	27.0	1.3	19.6
Coal (C)	1392	1.2	0.45	1.1	24.0	0.4	3.4

**Fig. 9** Ground reaction curves for horseshoe (HS) and inverted arch (IA) tunnels at strength of 37.5 % (normalized stress is the ratio of applied stress to the internal/in situ stress)

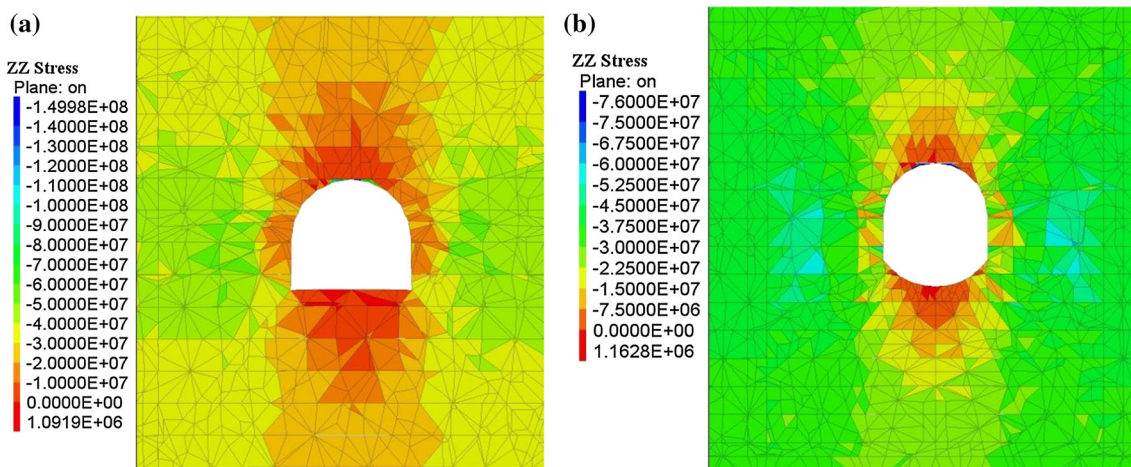
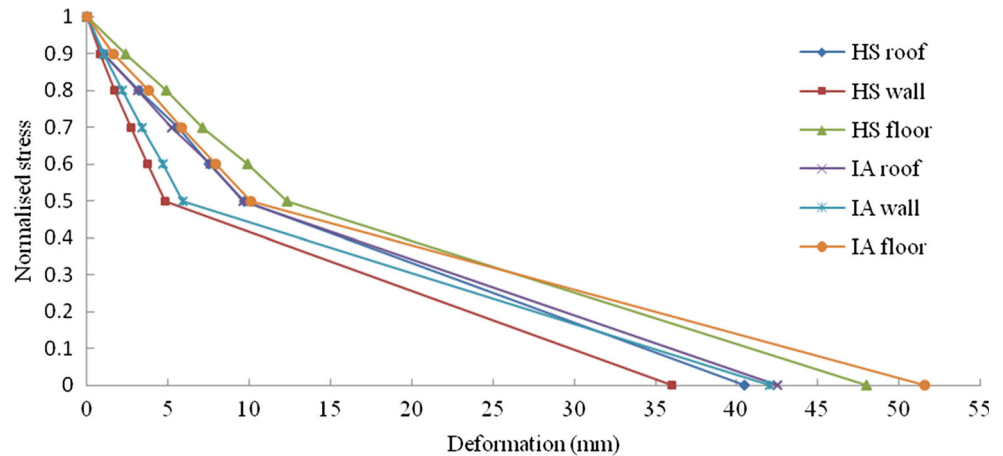


**Fig. 10** zz stress distribution around the excavation for a HS and b IA tunnels (unit: Pa)

In Fig. 9, the supports are installed at the normalized stress of 0.5. Due to the presence of explicit bedding planes, the rock mass properties estimated in this study are higher than what they would actually be. The bedding planes have, however, been added to study the support response. Towards this goal, a new technique using RStudio (Racine 2012) has been adopted to estimate support factor of safety. RStudio is an environment for the R statistical programming language. Cables in 3DEC are discretized into smaller elements called segments and the axial forces are made available for each ‘segment.’ Hence, this cannot directly be used to calculate the factor of safety of the whole system. Each cable has been discretized into eight segments for this study. This produced more than 12,000 data points. To reduce the time and effort taken for computing the factor of safety, it was decided to use RStudio. For each cable, the highest axial force out of the eight segments was recorded and averaged over all cables of a particular type to estimate the factor of safety. While this does not provide information on the failure of any

isolated cable, it provides an accurate status of the tunnel as a whole. Similarly, grout bonds can either be intact or broken. The grout bond failure percentage has been calculated as the number of broken bonds as a percentage of total number of bonds for a specific cable type.

Figures 10 through 16 show the plots of various results from 3DEC for the horseshoe and inverted arch tunnels at 37.5 % strength. The results are not shown for all the cases to avoid repetition. It can be seen from Figs. 10 and 11 that the zz and xx stresses approach zero at locations close to roof and floor, and walls, respectively, as one would intuitively expect. Note that the peak stresses are observed at a slight distance away from the opening as opposed to at the excavation boundary. This is due to joint separation which has caused stress relaxation close to the excavation. Figures 12 and 13 show the deformation distributions where significant deformations can be distinctly observed around the walls, sagging roof, and some degree of floor heaving around the tunnels. The thickness of the failure zone is shown in Fig. 14. The suffix ‘p’ in shear-p and tension-p



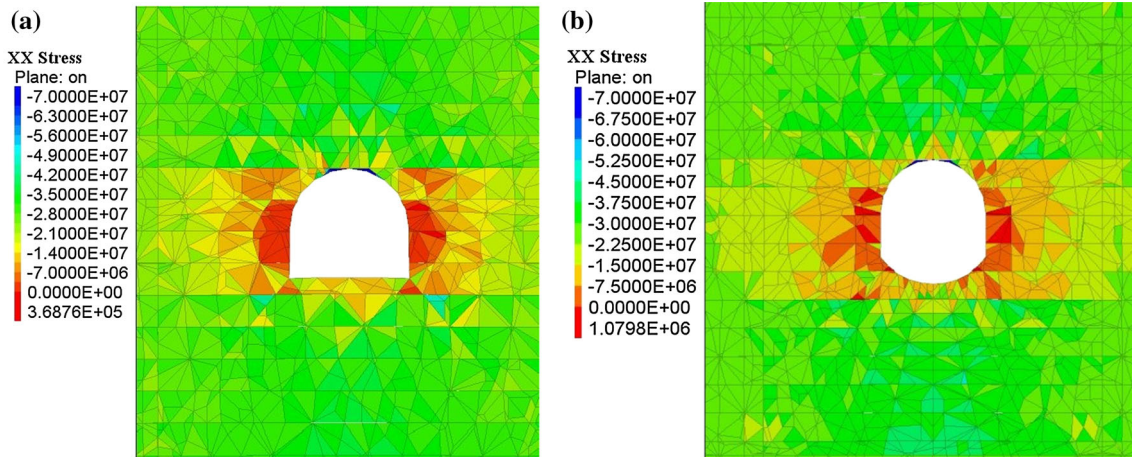


Fig. 11 xx stress distribution around the excavation for a HS and b IA tunnels (unit: Pa)

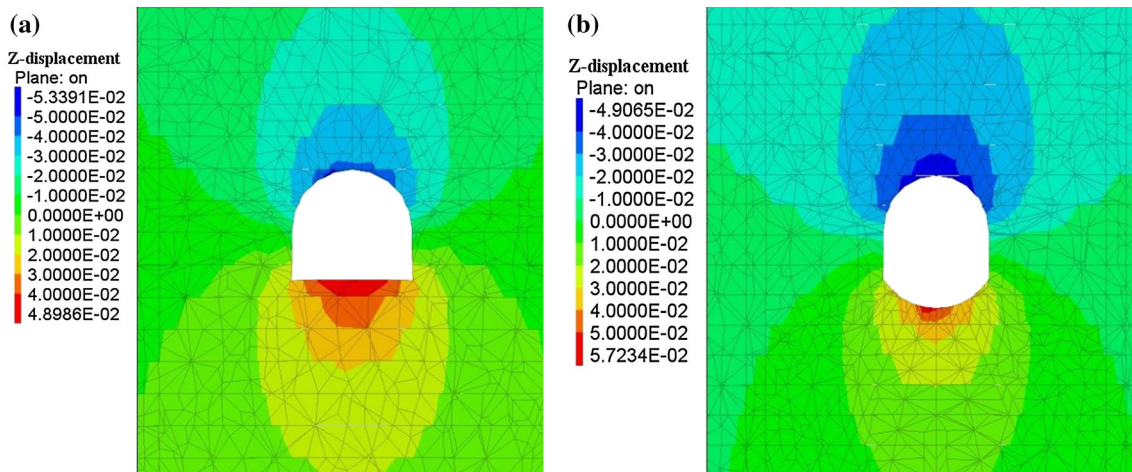


Fig. 12 Vertical displacement distribution around the excavation for a HS and b IA tunnels (unit: m)

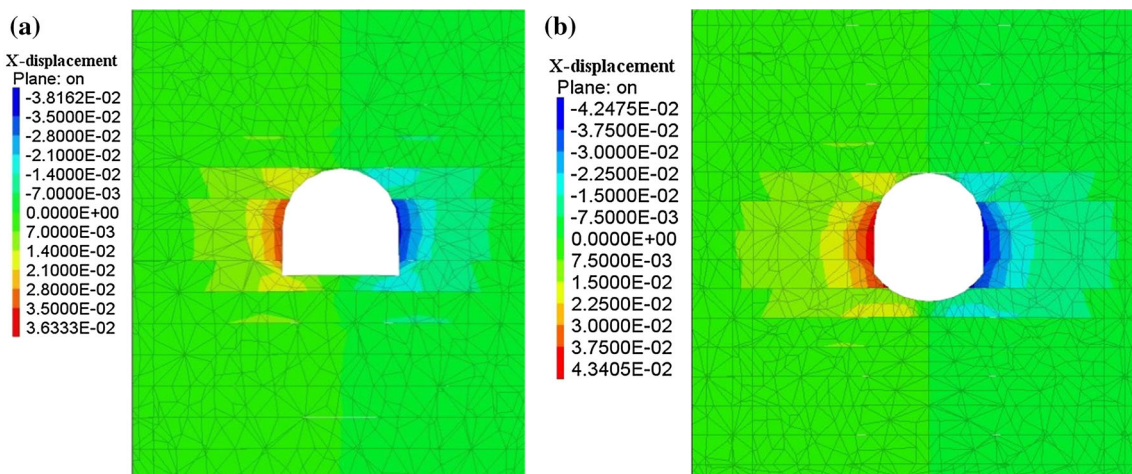


Fig. 13 Horizontal displacement distribution around the excavation for a HS and b IA tunnels (unit: m)

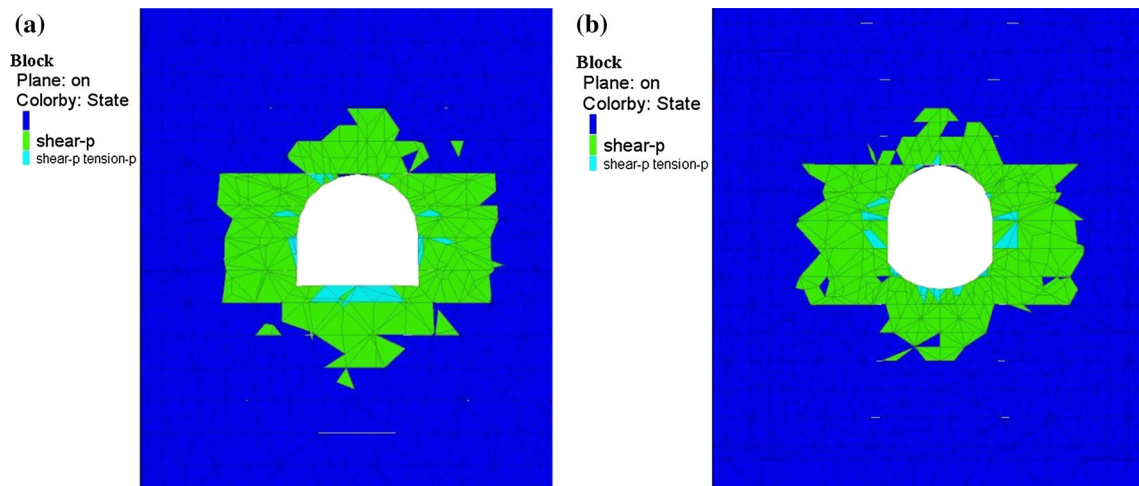


Fig. 14 Failure zone status around the excavation for a HS and b IA tunnels

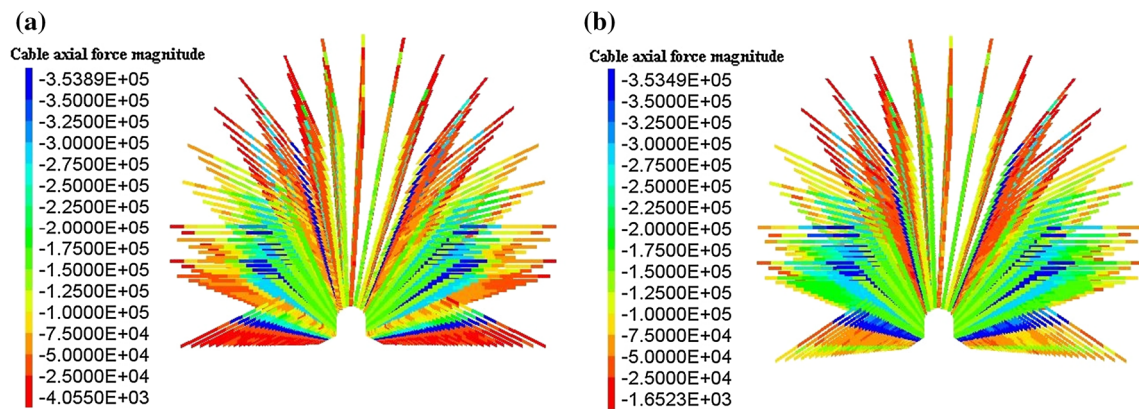


Fig. 15 Axial force distribution for cable elements in a HS and b IA tunnels (unit: N)

stands for past. The interpretation is that the region corresponding to the shear-p color has undergone shear failure in the past, i.e., some time prior to attaining the equilibrium state, and so on. Figures 15 and 16 show the status of the two cable parameters—ultimate tensile capacity and grout bond strength. It can be observed that the highest axial force in the cable is about 353.9 kN which is dangerously close to the ultimate strength of 354 kN. Hence, despite the average factor of safety being above 1.0, there is possibility of local failure of some cables. The segments which have the broken bond status are also the segments which appear to undergo highest axial loading. This provides an indication of the location of highest likelihood of failure for the cables.

Figures 17 through 24 summarize graphically the results presented in Tables 7, 8, 9, and 10. Figures 17 and 18 give the roof, wall, and floor deformations for the two tunnel systems obtained using the instantaneous supporting and stress relaxation methods. Also included in Figs. 17 and 18

are the field deformation measurements in the form of the vertical dotted lines and the corresponding calibrated rock mass property values through the horizontal lines. It can be seen that the deformations obtained through both methods are very similar for strengths higher than 30 %. For strengths lower than 30 %, the instantaneous support installation yields lower deformations. Figures 19 and 20 depict the relation between support factor of safety and rock mass strength. As intuitively expected, the factor of safety reduces with decrease in rock mass strength and tends to unity. In both tunnels, the first support has a higher factor of safety up to strength of about 50 %. This indicates an unbalanced load sharing between the two supports with the second support carrying significantly higher load. Below 50 % strength, this feature is reversed but the load sharing is more or less equal. Due to delayed installation, the rock mass undergoes stress relaxation as a result of which the support factor of safety is higher. This effect is especially prominent at higher strengths –2.79 versus 4.07



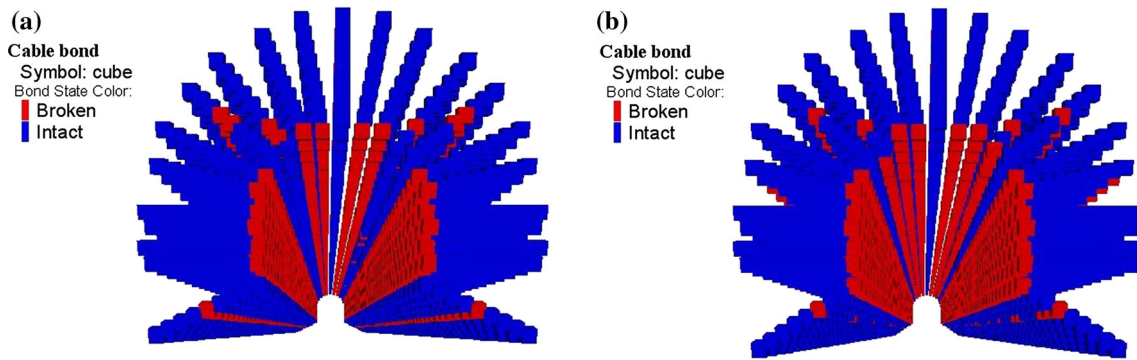
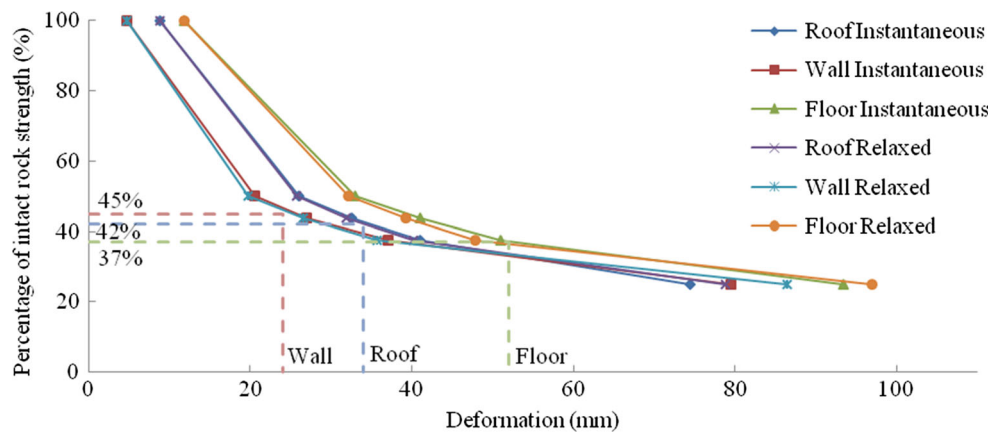


Fig. 16 Cable bond status for cable elements in a HS and b IA tunnels

Fig. 17 Horseshoe tunnel deformations as a function of rock mass strength (instantaneous and relaxed are the two support installation mechanisms; the three vertical lines and the corresponding horizontal lines show the field deformation measurements and the corresponding calibrated rock mass properties, respectively.)



for horseshoe and 2.68 versus 4.53 for inverted arch. While this difference between the two installation techniques significantly reduces at lower strengths, it is still a good marker to estimate a range of possible factors of safety between a worst-case (instantaneous installation) and a best-case (delayed installation) scenario. It can be observed from Figs. 21 and 22 that the grout bond failures follow a similar trend with failure increasing with reduced rock mass strength. For a given rock mass strength, the failures are also lower for the delayed installation as compared to instantaneous installation for rock mass strengths greater than 50 %. In Figs. 21 and 22, the grout failures have been divided into those for first and second supports separately. Note that the load sharing % between the two support types can be different. Accordingly, a possibility exists for grout failure % to decrease with decreasing rock mass strength for each support system by sharing a lower load. It was observed that such an anomaly appears to have taken place in Fig. 21 in the second support system under both instantaneous and relaxed support conditions when the rock mass strength was decreased from 50 to 37.5 % of the intact rock strength.

Once calibrated, the models were used to carry out the necessary analyses described in Table 1. A summary of

results from the analyses is given in Table 12. Normal bolting is been used to refer to roof and wall bolting, whereas floor bolting is used to indicate that the floor has been bolted in addition to the roof and walls.

An immediately obvious observation that can be made from the results in Table 12 is that the yield zone in most of the cases is close to the cable lengths of 2.2 and 2.5 m. This provides very little bond area for the grout. Hence, a set of analyses were performed to observe whether longer cables would work more efficiently since they would likely have more cable length for anchorage. Towards this objective, cable lengths of 3.5 and 4.0 m were selected for the first and second supports, respectively. Results of analyses carried out using these lengths are presented in Table 13. The long bolts were applied on the roof, walls, and floor of the tunnels.

Figures 23 and 24 graphically show the behavior of the horseshoe and inverted arch tunnel deformations under different bolting conditions. Compared to the unsupported cases, normal bolting helps reduce roof and wall deformations by up to 15 %. However, as one would expect, it has moderate effect on floor deformations. On bolting the floor in addition to roof and walls, the floor deformations reduce by 15 and 10 % in the horseshoe and inverted arch

**Fig. 18** Inverted arch tunnel deformations as a function of rock mass strength (instantaneous and relaxed are the two support installation mechanisms; the *three vertical lines* and the corresponding *horizontal lines* show the field deformation measurements and the corresponding calibrated rock mass properties, respectively.)

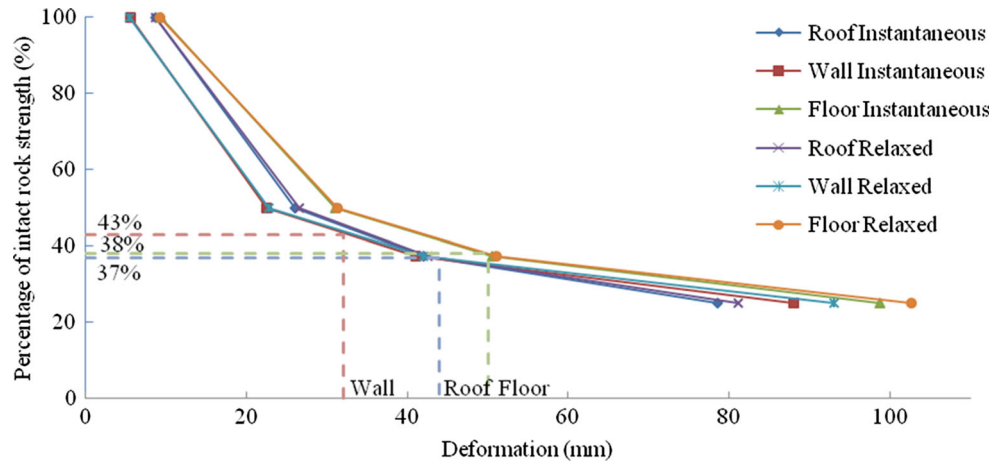


**Fig. 19** Horseshoe tunnel support factor of safety as a function of rock mass strength (instantaneous and relaxed are the two support installation mechanisms). Due to truncation of the figure to provide better resolution, the factor of safety at rock mass strength of 100 % intact rock strength is not available for all curves. Instead, the rock mass strength value at the truncated factor of safety of 3.0 is provided next to each curve

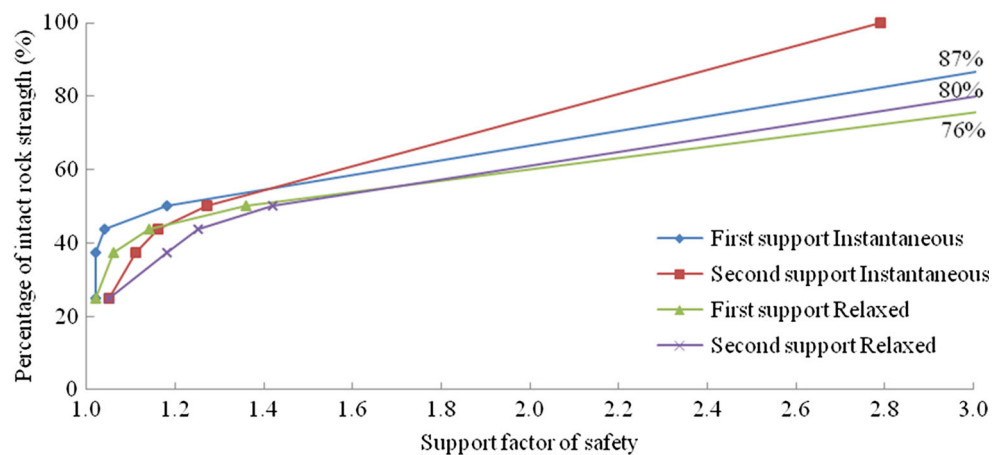
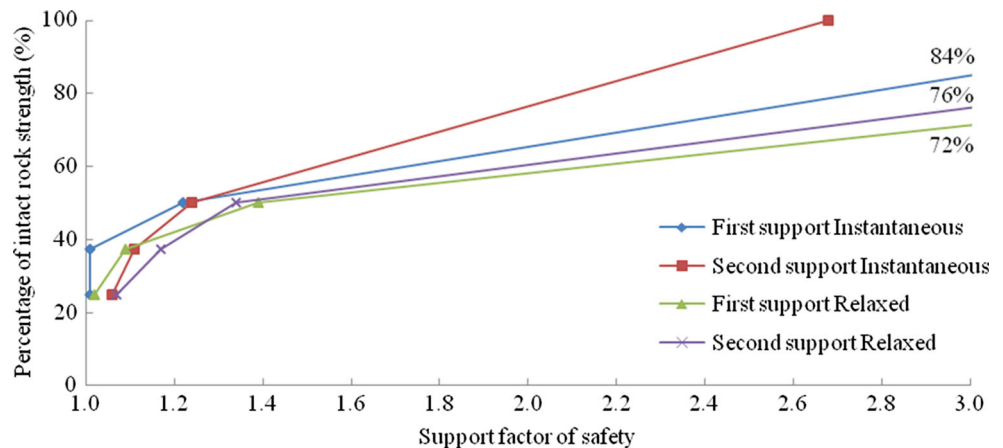


**Fig. 20** Inverted arch tunnel support factor of safety as a function of rock mass strength (instantaneous and relaxed are the two support installation mechanisms). Due to truncation of the figure to provide better resolution, the factor of safety at rock mass strength of 100 % intact rock strength is not available for all curves. Instead, the rock mass strength value at the truncated factor of safety of 3.0 is provided next to each curve



tunnels. The deformations appear to be largely unaffected by the length of the bolt and mode of bolt installation (instantaneous or delayed). However, the effect of increasing the cable length is especially observed in Table 13 through the improved cable factor of safety and reduced bond failures. While the longer cables have caused the factor of safety to increase by up to 14 % in case of the

horseshoe tunnel, they can also be seen to improve load sharing. This is seen from the more or less similar factor of safety values for the first and second supports (1.31 vs. 1.34, 1.12 vs. 1.12 etc.). The grout bond failures have nearly reduced by half from 15 to 6–7 % due to the use of longer cables. In some cases such as the inverted arch tunnel with delayed support installation, the size of yield

**Fig. 21** Horseshoe tunnel cable grout bond failure as a function of rock mass strength (instantaneous and relaxed are the two support installation mechanisms). Note that the anomaly appearing in the figure around the grout bond failure of 10–12 % is explained in the text

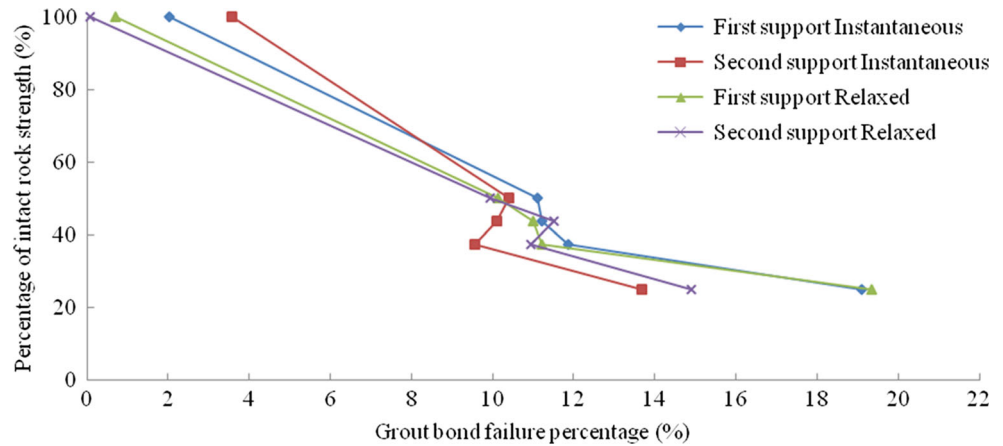


**Fig. 22** Inverted arch tunnel cable grout bond failure as a function of rock mass strength (instantaneous and relaxed are the two support installation mechanisms)

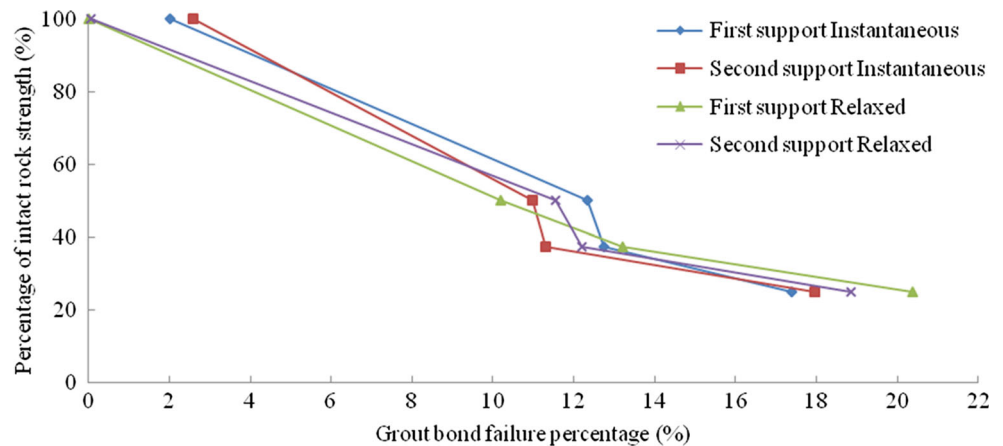


**Table 12** Summary of analyses carried out on the calibrated model

Case	Deformation (mm)			Factor of safety		Grout bond failure (%)		Yield zone (m)		
	Roof	Wall	Floor	First support	Second support	First support	Second support	Roof	Wall	Floor
1-HS unsupported	34.5	30	42.5					2.1	2.3	2.6
2-HS, I, normal	32.5	27	41	1.04	1.16	11.22	10.10	2	2.3	2.6
3-HS, I, floor	32	27	36.8	1.08	1.12	13.52	14.54	2	2.1	2.5
4-HS, SR, normal	31.9	26.6	39.3	1.14	1.25	11.01	11.50	1.5	2	2.1
5-HS, SR, floor	31.8	27	36.8	1.18	1.22	10.17	11.08	1.5	2	1.5
6-IA unsupported	45	47	52					2.1	3.2	2.6
7-IA, I, normal	42	41	50.5	1.01	1.11	12.73	11.31	2	3.2	2.7
8-IA, I, floor	41.5	40	47	1.02	1.09	12.20	11.40	2	3	2.2
9-IA, SR, normal	42.5	42	51	1.09	1.17	13.20	12.20	1.5	2.5	2.5
10-IA, SR, floor	42.5	41.5	46.8	1.05	1.13	16.00	12.30	1.5	2.6	2

HS horseshoe, IA inverted arch, I instantaneous supporting, SR stress relaxation

zone has reduced from 2.0 to 1.7 m in the floor due to the use of longer cables.

An important assessment is the selection of the right tunnel shape for the given situation. Since the tunnels in the mine are of different cross-sectional areas, it is not possible to directly decide on the best tunnel shape. Since the

inverted arch tunnel being used in the mine has a 30 % higher cross-sectional area, it is not surprising that it has undergone higher deformation. Hence, it has been attempted to normalize the deformations by considering the closure strains. A summary of closure strains for different deformations is given in Table 14 and Fig. 25. It may be

**Table 13** Analyses carried out using longer cable bolts

Case	Deformation (mm)			Factor of safety		Grout bond failure (%)		Yield zone (m)		
	Roof	Wall	Floor	First support	Second support	First support	Second support	Roof	Wall	Floor
HS, I	32	26.5	36	1.17	1.21	7.70	8.30	2	2.1	2.5
HS, SR	31.5	26	36.8	1.34	1.31	6.00	7.00	1.5	2	1.5
IA, I	41.4	39.7	46.4	1.07	1.09	7.78	8.35	1.9	2.8	2
IA, SR	42	41	46.6	1.12	1.12	7.62	7.15	1.2	2.5	1.7

HS horseshoe, IA inverted arch, I instantaneous supporting, SR stress relaxation

**Fig. 23** Effect of different bolting scenarios on horseshoe tunnel deformation

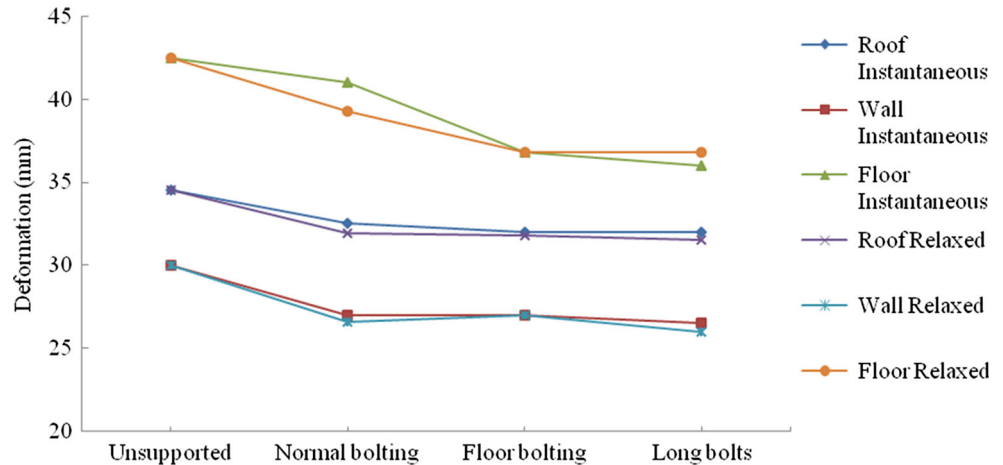
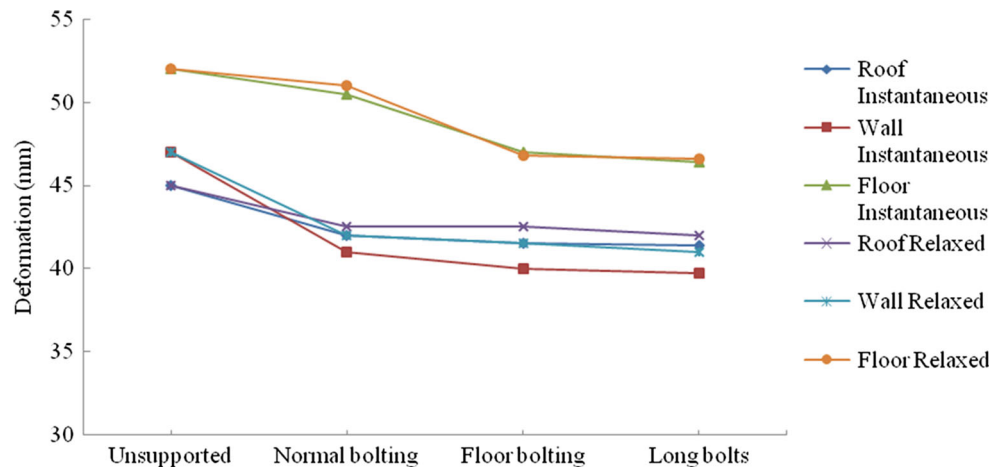


**Fig. 24** Effect of different bolting scenarios on inverted arch tunnel deformation



noted that the difference in closure strain between the two support installation procedures is negligible and has been ignored. Hence, the results have not been presented separately.

It can be seen from Table 14 and Fig. 25 that for a given rock mass strength, the horizontal closure strain for the inverted arch tunnel is higher than for the horseshoe tunnel although the difference is quite small. However, the vertical closure strain for the inverted arch tunnel is significantly lower than for the horseshoe shape. Hence, for the

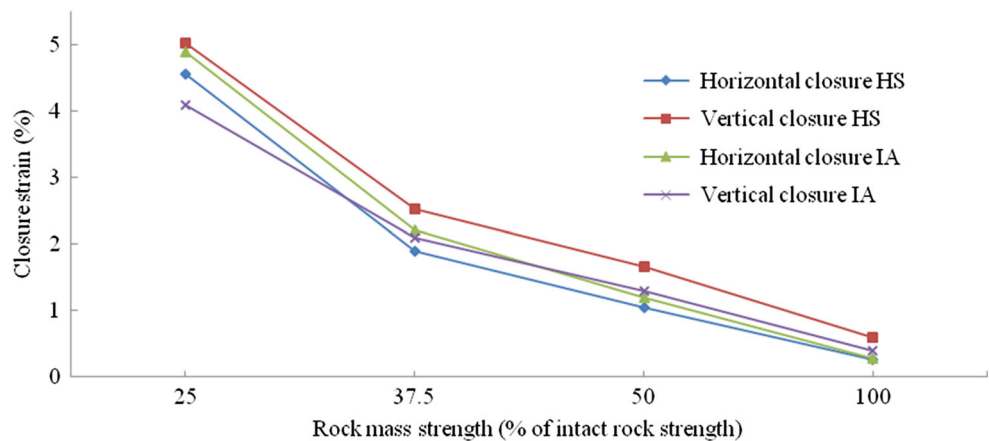
mine being studied, which is experiencing floor heave, the inverted arch shape may prove favorable.

### 5 Conclusions

Two deep tunnels in a coal-measure stratum, under a high in situ stress field, have been modeled using the distinct element method. Available data on in situ stress, tunnel geometry, joint orientation, joint and intact rock

**Table 14** Closure strains for the two tunnel shapes

Rock mass strength as a percentage of intact strength (%)	Horizontal closure strain (%)		Vertical closure strain (%)	
	Horseshoe	Inverted arch	Horseshoe	Inverted arch
100	0.25	0.28	0.59	0.40
50	1.04	1.19	1.65	1.28
37.5	1.89	2.21	2.53	2.09
25	4.55	4.89	5.02	4.09

**Fig. 25** Comparison of closure strains between the two tunnel shapes (*HS* horseshoe, *IA* inverted arch)

mechanical properties, and support properties have been fully incorporated into the model to back-analyze the rock mass mechanical properties using available field deformation data. Two methods of support installation have been used in the model calibration; one by immediately installing the supports after excavation and another by installing supports after allowing the rock mass around the excavation to undergo some stress relaxation as is the case in the field. Both methods point to a rock mass strength of about 35–45 % of the intact rock strength. Additionally, a new procedure has been developed to estimate the average factor of safety and grout failure of the support system using RStudio. The two methods of support installation have been observed to yield very similar deformations, but support factor of safety is higher and grout failures are lower when the stress relaxation based method is used. Analysis using both methods provides a range of possible support factors of safety and grout failures. The calibrated models have been analyzed using different support patterns and lengths, and without supports to better understand the role of supports in tunnel stability. It has been observed that the tunnel is most stable and suffers minimum deformations when supports are installed on the floor as well, in addition to the roof and walls. Since the fractured zone around tunnels were similar in size to the supports used, the models were analyzed by installing longer bolts of 3.5 and 4 m as opposed to the currently used 2.2 and 2.5 m long bolts. This resulted in improved factors of safety and lower

grout failure. Finally, a comparative study between the two tunnel shapes were carried out using the horizontal and vertical closure strains. The horseshoe tunnel had higher vertical closure strains and comparable horizontal closure strains with the inverted arch tunnel.

**Acknowledgments** The research was funded by the US Centers for Disease Control and Prevention under the Contract No. 200-2011-39886. The authors would like to thank Xiezhuan Coal Mine and Dr. Zhengxing Yu and Professor Fuxing Jiang of University of Science and Technology Beijing for providing laboratory and field geological and geotechnical data for this research. The authors further thank the Xiezhuan Coal Mine for providing the encouragement to conduct this research and to publish the research findings.

## References

- Aldorf J, Exner K (2013) Mine openings: stability and support. Elsevier, Oxford
- Barla G, Barla M (2000) Continuum and discontinuum modelling in tunnel engineering. *Min Geol Pet Eng Bull* 12:45–57
- Brown ET, Bray JW, Ladanyi B, Hoek E (1983) Ground response curves for rock tunnels. *J Geotech Eng* 109(1):15–39
- Cheng YM (1998) Advancements and improvement in discontinuous deformation analysis. *Comput Geotech* 22(2):153–163. doi:10.1016/S0266-352X(98)00002-0
- China Coal Society Open Pit Mine Committee (2010) China Open Pit Coalmining Development Report (1914–2007). China Coal Industry Publishing House, Beijing
- Coggan J, Gao F, Stead D, Elmo D (2012) Numerical modelling of the effects of weak immediate roof lithology on coal mine roadway stability. *Int J Coal Geol* 90:100–109



- Compiling Committee of China (2010) China Coal Industry yearbook 2009. China Coal Industry Press, Beijing
- Cundall PA (1971) A computer model for simulating progressive, large-scale movements in blocky rock systems. In: The international symposium on rock mechanics, 2, pp 47–65
- Cundall PA (2001) A discontinuous future for numerical modelling in geomechanics? *Proc ICE Geotech Eng* 149(1):41–47
- Deb D, Das KC (2010) Extended finite element method for the analysis of discontinuities in rock masses. *Geotech Geol Eng* 28(5):643–659
- Eberhardt E, Stead D, Coggan J, Willenberg H (2003) Hybrid finite-/discrete-element modelling of progressive failure in massive rock slopes. In: Handley M, Stacey D (eds) 10th Congress of the international society for rock mechanics (pp 275–280). Johannesburg: The South African Institute of Mining and Metallurgy. [http://www.eoas.ubc.ca/personal/erik/e-papers/03EE\\_ISRMCongress-Elfen.pdf](http://www.eoas.ubc.ca/personal/erik/e-papers/03EE_ISRMCongress-Elfen.pdf)
- Elmo D (2006) Evaluation of a hybrid FEM/DEM approach for determination of rock mass strength using a combination of discontinuity mapping and fracture mechanics modelling, with particular emphasis on modelling of jointed pillars. (Unpublished Ph.D. Dissertation). University of Exeter, Exeter UK
- Elmo D, Stead D (2010) An integrated numerical modelling–discrete fracture network approach applied to the characterisation of rock mass strength of naturally fractured pillars. *Rock Mech Rock Eng* 43(1):3–19
- Elmo D, Stead D, Eberhardt E, Vyazmensky A (2013) Applications of finite/discrete element modeling to rock engineering problems. *Int J Geomech* 13(5):565–580. doi:10.1061/(ASCE)GM.1943-5622.0000238
- Fairhurst C, Pei J (1990) A comparison between the distinct element method and the finite element method for analysis of the stability of an excavation in jointed rock. *Tunn Undergr Space Technol* 5(1–2):111–117. doi:10.1016/0886-7798(90)90066-S
- Ghee EH, Zhu BT, Wines DR (2006) Numerical analysis of twin road tunnels using two-and three-dimensional modelling techniques. In: Fourth International FLAC symposium on numerical modelling in geomechanics
- Hamdi P, Stead D, Elmo D (2014) Damage characterization during laboratory strength testing: a 3D-finite-discrete element approach. *Comput Geotech* 60:33–46. doi:10.1016/j.compgeo.2014.03.011
- Hao YH, Azzam R (2005) The plastic zones and displacements around underground openings in rock masses containing a fault. *Tunn Undergr Space Technol* 20:41–61. doi:10.1016/j.tust.2004.05.003
- He X, Song L (2012) Status and future tasks of coal mining safety in China. *Saf Sci* 50(4):894–898. doi:10.1016/j.ssci.2011.08.012
- Hoek E, Kaiser PK, Bawden WF (2000) Support of underground excavations in hard rock. CRC Press, Boca Raton
- Huang S (2008) China Coal Outlook 2009. China coal industry publishing house, Beijing
- Itasca (2008) 3DEC user's guide. Itasca Consulting Group Inc., Minnesota
- Jian-ping Z, Ren-ke W, Ai-min W, Yang L, Wang Z (2012) Optimization support controlling large deformation of tunnel in deep mine based on discontinuous deformation analysis. *Procedia Environ Sci* 12(Icese 2011):1045–1054. doi:10.1016/j.proenv.2012.01.386
- Kang Y, Liu Q, Gong G, Wang H (2014) Application of a combined support system to the weak floor reinforcement in deep underground coal mine. *Int J Rock Mech Min Sci* 71:143–150
- Kulatilake PHSW, Ucpirtti H, Wang S, Radberg G, Stephansson O (1992) Use of the distinct element method to perform stress analysis in rock with non-persistent joints and to study the effect of joint geometry parameters on the strength and deformability of rock masses. *Rock Mech Rock Eng* 25(4):253–274
- Kulatilake PHSW, Wang S, Stephansson O (1993) Effect of Finite Size Joints on the deformability of jointed rock in three dimensions. *Int J Rock Mech Min Sci Geomech Abstr* 30(5):479–501
- Kulatilake PHSW, Park J, Um JG (2004) Estimation of rock mass strength and deformability in 3-D for a 30 m cube at a depth of 485 m at Äspö hard rock laboratory. *Geotech Geol Eng* 22(3):313–330
- Lisjak A, Grasselli G, Vietor T (2014) Continuum-discontinuum analysis of failure mechanisms around unsupported circular excavations in anisotropic clay shales. *Int J Rock Mech Min Sci* 65:96–115. doi:10.1016/j.ijrmmms.2013.10.006
- Ma YM (1999) Development of discontinuous deformation analysis the first 10 years (1986–1996). In: Proceedings third international conference on analysis of discontinuous deformation, Vail, Colorado, USA, pp 17–32
- Macklin SR, Varley P, Varona P, Merino C (2012) The investigation and design for a unique architectural space—the Chillida Cavern, Mount Tindaya, Fuerteventura. *Tunn Undergr Space Technol* 31:9–19. doi:10.1016/j.tust.2012.04.001
- MacLaughlin MM, Doolin DM (2006) Review of validation of the discontinuous deformation analysis (DDA) method. *Int J Numer Anal Meth Geomech* 30(4):271–305. doi:10.1002/nag.427
- Mahabadi OK, Lisjak A, Munjiza A, Grasselli G (2012) Y-Geo : new combined finite-discrete element numerical code for geomechanical applications. *Int J Geomech* 12(6):676–688. doi:10.1061/(ASCE)GM.1943-5622.0000216
- Mark C, Barczak TM (2000) Fundamentals of coal mine roof support. In: New Technology for Coal Mine Roof Support, Proceedings of the NIOSH open industry briefing, NIOSH IC, vol 9453. pp 23–42
- Munjiza A, Owen DRJ, Bicanic N (1995) A combined finite-discrete element method in transient dynamics of fracturing solids. *Eng Comput* 12(2):145–174
- Ohnishi Y, Sasaki T, Koyama T, Hagiwara I, Miki S, Shimauchi T (2014) Recent insights into analytical precision and modelling of DDA and NMM for practical problems. *Geomech Geoeng* 9(2):97–112
- Peng SS, Tang DHY (1984) Roof bolting in underground mining: a state-of-the-art review. *Int J Min Eng* 2(1):1–42
- Price DG (2008) In: De Freitas MH (ed) Engineering geology: principles and practice. Springer, Berlin
- Racine JS (2012) RStudio: a platform-independent IDE for R and Sweave. *J Appl Econom* 27(1):167–172
- Rockfield Software Ltd (2011) Elfen User manual. Swansea, UK
- Scheldt T (2003) Comparison of continuous and discontinuous modelling for computational rock mechanics. Doctoral Dissertation, Norwegian University of Science and Technology
- Shan XY, Mei HB, Xu DQ, Zhao YX (2005) Mining-induced influences on stability of floor haulage roadway in tectonic stress field. *Yanshilixue Yu Gongcheng Xuebao/Chin J Rock Mech Eng* 24(12):2101–2106
- Shi G (2007) Applications of discontinuous deformation analysis (DDA) to rock engineering. In: International seminar on computational mechanics (ISCM 2007) (pp 136–147)
- Shi GH (2014) Application of discontinuous deformation analysis on stability analysis of slopes and underground power houses. *Geomech Geoeng* 9(2):80–96. doi:10.1080/17486025.2013.871065
- Shi GH, Goodman RE (1985) Two dimensional discontinuous deformation analysis. *Int J Numer Anal Meth Geomech* 9(6):541–556. doi:10.1002/nag.1610090604

- Singh R, Mandal PK, Singh AK, Singh TN (2001) Cable-bolting-based semi-mechanised depillaring of a thick coal seam. *Int J Rock Mech Min Sci* 38(2):245–257
- Vardakos SS, Gutierrez MS, Barton NR (2007) Back-analysis of Shimizu Tunnel No. 3 by distinct element modeling. *Tunn Undergr Space Technol* 22(4):401–413. doi:[10.1016/j.tust.2006.10.001](https://doi.org/10.1016/j.tust.2006.10.001)
- Vyazmensky A, Elmo D, Stead D (2010) Role of rock mass fabric and faulting in the development of block caving induced surface subsidence. *Rock Mech Rock Eng* 43(5):533–556
- Wang X, Kulatilake PHSW, Song WD (2012) Stability investigations around a mine tunnel through three-dimensional discontinuum and continuum stress analyses. *Tunn Undergr Space Technol* 32:98–112
- Wu Q, Kulatilake PHSW (2012) Application of equivalent continuum and discontinuum stress analyses in three-dimensions to investigate stability of a rock tunnel in a dam site in China. *Comput Geotech* 46:48–68
- Wu JH, Ohnishi Y, Shi G, Nishiyama S (2005) Theory of three-dimensional discontinuous deformation analysis and its application to a slope toppling at Amatoribashi, Japan. *Int J Geomech* 5(3):179–195
- Xiao TQ, Bai JB, Wang XY, Chen Y, Yu Y (2011) Stability principle and control of surrounding rock in deep coal roadway with large section and thick top-coal. *Rock Soil Mech* 32(6):1874–1880
- Yuyong J, Jian Z (2004) On using DEM for simulating response of jointed rock to underground explosion. *Chin J Rock Mech Eng* 23(2):5
- Zhao ZY, Bao HR, Tian Q (2011) On the complementation of augmented Lagrangian method in the 2D discontinuous deformation analysis. In: Zhao J, Ohnishi Y, Zhao GF, Sasaki T (eds) *Advances in discontinuous numerical methods and applications in geomechanics and geoengineering, ICADD10*, HA. CRC Press, pp 181–187